Cobaloxime tethered pyridine-functionalized ethylene-bridged periodic mesoporous organosilica as efficient HER catalyst

M[a] Ángeles Navarro,[a] Daniel Cosano,[a] Asamanjoy Bhunia,[b] Laura Simonelli,[c] Vlad Martin-Diaconescu,[c] Francisco J. Romero-Salguero[a*] and Dolores Esquivel[a]*

[a]Department of Organic Chemistry, Nanochemistry and Fine Chemistry Research Institute (IUIQFN), Faculty of Sciences, University of Córdoba, Campus de Rabanales, Marie Curie Building, Ctra. Nnal. IV, km 396, 14071 Córdoba, Spain.

[b]Department of Chemistry, Inorganic Chemistry Section, Jadavpur University, Kolkata 700032, India

[c]ALBA Synchrotron Light Facility, Carrer de la Llum 2-26, 08290 Cerdanyola del Vallès, Spain

*q02rosaf@uco.es (F.J.R.-S.); q12esmem@uco.es (D.E.)

ABSTRACT

An efficient cobaloxime hydrogen production catalyst has been synthesized through coordination of a cobalt complex ($Co(dmgH_2)(dmgH)Cl_2$) on an ethylene-bridged periodic mesoporous organosilica (PMO) containing pyridine moieties. The effective assembly of cobaloxime units through cobalt-pyridine axial bond on the porous channels of the PMO was clearly evidenced by different techniques, including ^{13}C NMR, Raman, IR and XPS. The catalyst was investigated for the hydrogen evolution reaction in a visible-light activated system in the presence of a photosensitizer (eosin Y) and a sacrificial electron donor (TEOA). It showed a good photocatalytic performance on the HER with a TON of 119 at 6 h, largely exceeding the catalytic activity of the homogeneous counterpart, $Co(dmgH)_2pyCl$, under the conditions studied. The process was proven to be photocatalytic and heterogeneous. The studied system has the cobaloxime catalyst with the highest turnover reported to date for a heterogeneous catalyst under photocatalytic conditions. This catalytic system maintained its activity after two recycling experiments, previous activation of the catalyst.

Keywords: cobaloxime; axial pyridine ligand; periodic mesoporous organosilicas; hydrogen evolution reaction.

Introduction

In response to the dramatic increase of atmospheric levels of CO_2 due to the worldwide strong dependence on fossil fuels to obtain energy, scientists have been working on the development and implementation of sustainable carbon-free energy sources.[1]

Among them, solar energy is by far the most feasible and promising alternative to carbon-fuels. Theoretically, the incident solar energy on the earth every hour is more than enough to satisfy all energy demanded by humans for the entire year.[2,3] Despite electricity generation from the sun using photovoltaic cells currently contributes more than 3.5% of the world's electricity[4], there exists barriers to the complete implementation of solar energy. The daily and seasonal fluctuations of solar flux along with the absence of methods for storing and dispatching on demand have not allowed its development as the major primary energy source.

Alternatively, an interesting approach inspired by natural photosynthesis is solar driven water-splitting, able to store energy in chemical bonds (H_2 and O_2).[5,6] As a result of the well-known complications in driving both half-reactions,[7] most of the studies have been focused on the reductive side of water splitting to obtain hydrogen as an energy vector. However, a hydrogen economy requires the design of cost-effective and efficient catalysts for hydrogen production through an economically viable process. In this context, molecular catalysts based on earth-abundant element (Co, Ni and Fe) complexes are playing an important role for water splitting.[8] Particularly, cobalt-based compounds have emerged as efficient molecular systems for both water oxidation[9,10] and hydrogen evolution reactions[11,12] in the last decade. Specifically, cobaloxime (cobalt bis-glyoximato complexes) compounds are among the most widely studied for electro- and photocatalytic hydrogen production due to their facile synthesis and tunable catalytic

properties. These systems show high activity for proton reduction in aqueous solution at low overpotential.[13–17]

Since the pioneering studies by Ziessel and co-workers in this field,[18] numerous breakthroughs have been made in the design of efficient cobaloxime-based molecular systems for electro- and photocatalytic hydrogen evolution reaction (HER).[19,20] One of the most versatile approaches to improve electrocatalytic HER activity of cobaloximes is their immobilization on electroactive surfaces containing pyridine ligands. It is well documented by experimental[21–24] and computational[25–27]studies that the presence of aromatic N-donor group substituents in the axial position increases the catalytic efficiency of cobaloximes on hydrogen evolution. During the last decade, Reisner[28,29] and Artero[30,31] have led the research in this field, achieving good electrocatalytic HER activities with cobaloxime catalysts integrated into carbon-based nanomaterials. Recently, similar studies have been extended to other semiconductor substrates where H_2 production cobaloxime catalysts have been successfully assembled on electrode surfaces.[32,33] Another interesting approach involves immobilizing cobaloxime units on non-conducting surfaces for H_2 evolution under light-driven conditions. To the best of our knowledge, only MOFs (Metal Organic Frameworks) and, more recently, COFs (Covalent Organic Frameworks) have been employed as support for this purpose. Ott et col.[34] reported the first example of anchoring a cobaloxime catalyst onto chloromethylated MIL-101(Cr) for photocatalytic H_2 production. Recently, this research group has successfully integrated cobaloxime as metallo-linkers for MOF synthesis and has demonstrated that this system can act as electrocatalyst for extended periods of time.[35] In the field of COFs, Lotsch et col.[36] immobilized a cobaloxime catalyst on propargyl-functionalized COF-42 for HER. This stategy improved the photocatalytic activity of the cobaloxime compared with equivalent unbound cobaloxime.

As an alternative to these previous porous supports, periodic mesoporous organosilicas (PMOs) are a different family of hybrid materials with a great potential to immobilize molecular catalysts. The framework of PMOs is more hydrophobic than that of silicas and renders PMOs with a higher hydrothermal stability.[37] In addition, the well-defined ordered mesostructure, characteristic of these materials, facilitates the diffusion and accessibility of the reactants to the active centers.[38]

PMOs, prepared from organo-bridged alkoxysilane precursors in the presence of a surfactant, are characterized by highly ordered structures with organic groups homogenously distributed in the silica framework. A wide variety of organic groups has been successfully integrated in the silica walls of PMOs for applications such as catalysis, adsorption, chromatography, drug release and luminescence, among others[39–42]. One of the advantages of this synthetic stategy is the possiblity to incorporate different functional organic groups in the silica walls and the channel pores of the PMOs to provide attachment points for assembling homogenous catalysts. Recently, an example of it was reported by Inagaki et col. who incorporated a [FeFe]-hydrogenase model complex on the pore surface of a periodic mesoporous organosilica containing thiols groups to make an efficient heterogeneous HER catalyst. The material showed a greater TON than the homogenous system due to the improvement of the stability of the [FeFe]-complex on the pore surface of the PMO.[43] Taking this into consideration, PMOs with appropriate functional groups in their framework could act as excellent scaffolds for assembling other HER catalysts. Inmobilizing cobaloxime molecular complexes within PMO-supports with high surface areas and porous structures of a tailored hydrobicity/hydrophility could increase the stability of the cobaloxime catalyst confined into de mesopores and allow the easy catalyst recycling by filtration.

Herein, we report for the first time the incorporation of a cobaloxime catalyst [Co(dmgH_2)(dmgH)Cl_2] on the pore surface of an ethylene-bridged periodic mesoporous organosilica containing pyridine groups. The pyridine groups located at the pore channels provide attachment points to assemble cobaloxime catalysts on the surface PMO. The resulting material, py-etPMO-Co, was fully characterized and investigated for the photocatalytic HER. It showed to be a very efficient catalyst for hydrogen production, largely exceeding the photocatalytic activity of the homogeneous catalyst under the same conditions.

Experimental Section

Chemicals

Dimethylglyoxime (99%, Aldrich), cobalt (II) chloride hexahydrate (Acros Organics) and acetone (Aldrich) were used in the synthesis of cobaloxime complex. Octadecyltrimethylammonium bromide (ODTMA, Aldrich) and sodium hydroxide (NaOH, 99% Aldrich) were used as supplied. The organosilica precursors, *1,2-bis(triethoxysilyl)ethane* (97%) and *2-(4-pyridilethyl)triethoxysilane)* (95%), were obtained from abcr for the synthesis of pyridine-functionalized ethylene-bridged PMO. Both precursors were used as purchased without further purification. Acetonitrile (99.7%, PanReac), eosin Y (>95%, TCI) and triethanolamine (TEOA, >99% Sigma-Aldrich) were used for the photocatalytic hydrogen evolution reaction.

Synthesis procedures

Synthesis of cobaloxime complexes [Co(dmgH$_2$)(dmgH)Cl$_2$ and Co(dmgH)$_2$pyCl]

Cobaloxime complex, Co(dmgH$_2$)(dmgH)Cl$_2$, was synthesized according to a procedure previously reported.[44] In a typical synthesis, CoCl$_2$.6H$_2$O (0.5 g, 2.1 mmol) was dissolved in acetone (15 mL) and then, dimethylglyoxime (0.49 g, 4.2 mmol) was added. The resulting mixture was stirred for 10 min at room temperature. Afterwards, the mixture was filtered to remove any undissolved reactive. The filtrate was allowed to stand overnight to form green crystals. They were collected by filtration and washed with acetone. Co(dmgH$_2$)(dmgH)Cl$_2$ was dried under vacuum at 80 ºC. For the synthesis of the cobaloxime with axial pyridine ligand, Co(dmgH$_2$)(dmgH)Cl$_2$ (0.33 g, 0.9 mmol) was suspended in chloroform (8.5 mL) and then, pyridine (0.18 g) was added dropwise (Scheme 1).[44] Afterwards, water (3 mL) was added to the solution and stirring continued for 2 h. The aqueous phase was separated by decantation, while the organic phase was washed with three portions of water (15 mL each). The solution was concentrated by rotary evaporation and a precipitate was obtained by addition of ethanol. The final product was recovered by filtration, washed with ethanol, and dried under vacuum at 100 ºC.

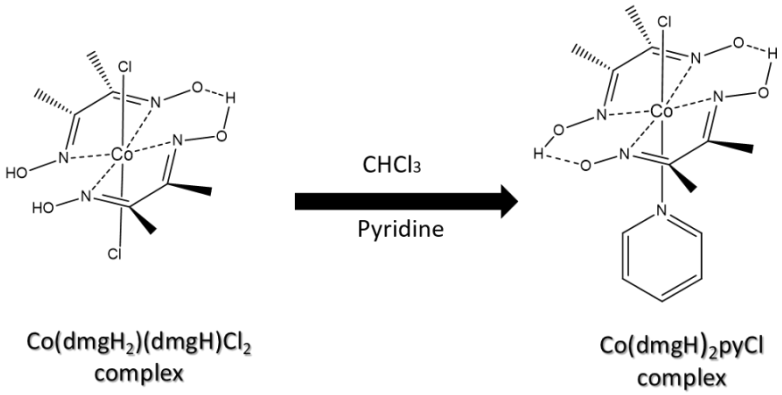

Scheme 1. Structures of cobaloxime complexes.

Synthesis of pyridine-functionalized ethylene-bridged PMO (py-etPMO)

In a typical synthesis,[45] ODTMA surfactant (0.85 g) was dissolved in a solution of NaOH (6 M, 0.89 mL) and distilled water (53 mL). After stirring the solution at room temperature for 24 h, a mixture of organosilane precursors with molar ratio 80% of 1,2-bis(triethoxysilyl)ethane and 20% of 2-(4-pyridylethyl)triethoxysilane was added dropwise under vigorous stirring. The resulting mixture was stirred at room temperature for 24 h, after which it was aged at 97 ºC for 48 h under static conditions. The white precipitate was recovered by filtration and washed with distilled water. To remove the surfactant, 1 g of as-synthesized material was refluxed in a solution containing 50 mL ethanol and 1 mL HCl solution (37% wt.) for 12 h. After repeating this extraction process twice, the final material was filtered out and dried at 120 ºC under vacuum. It was named *py-etPMO*.

Anchoring of cobaloxime catalyst Co(dmgH$_2$)(dmgH)Cl$_2$ on py-etPMO.

The material py-etPMO (0.5 g) was dispersed in 10 mL of methanol and then, Co(dmgH$_2$)(dmgH)Cl$_2$ complex (0.546 mmol) was added.[46] The mixture was kept under stirring at 65 ºC for 24 h. Subsequently, the solid was recovered by filtration and washed thoroughly with CH_3OH. To remove unreacted complex, the resulting solid was refluxed with 50 mL of CH_3OH for 12 h. This procedure was repeated twice. Finally, the solid was washed with DMSO, collected by filtration and dried under vacuum at 80 ºC. The catalyst was named *py-etPMO-Co.* A schematic illustration of the synthetic procedure of the cobaloxime-PMO hybrid material (py-etPMO-Co) is depicted in Scheme 2.

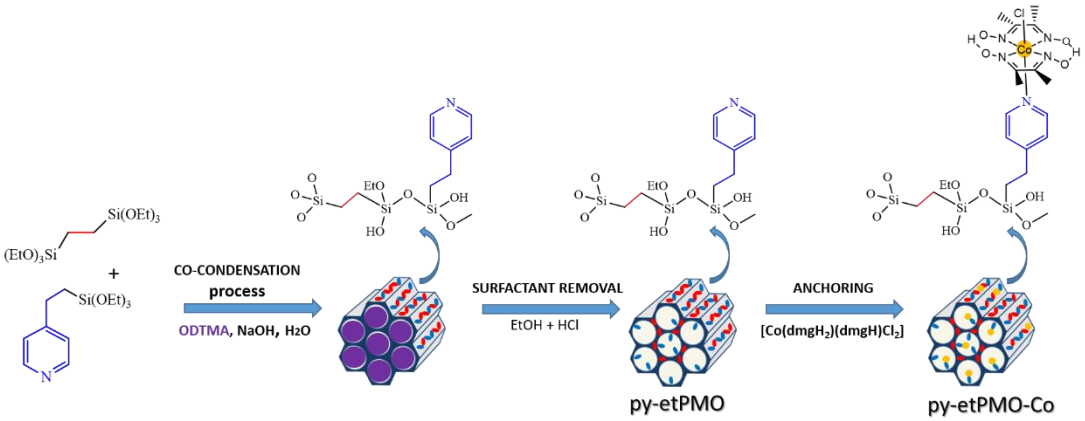

Scheme 2. Synthesis route of cobaloxime-PMO hybrid catalyst (py-etPMO-Co).

Photocatalytic studies

For the photocatalytic experiment, py-etPMO-Co (1 mg) was suspended in a CH_3CN:H_2O (1:1) solution (11.4 mL). The aqueous solution contains triethanolamine (TEOA, 10%) adjusted to pH 7 with HCl (37 %) and the acetonitrile solution contains dissolved Eosin Y (0.05 mM). The reaction tube was sealed, and the mixture was purged with N_2 for 30 min. Then, the reaction mixture was irradiated with a Xe lamp (ORIEL, 300 W) equipped with (Newport filter, FSQGC400) at a distance of 10 cm. Sample aliquots were taken using a gas-tight syringe and quantified by gas chromatography (Shimadzu GC-2010 Plus) equipped with a barrier discharge ionization detector (BID) and a ShinCarbon ST column (2 m × 2 mm i.d.). For the homogenous test, [Co(dmgH)$_2$pyCl] was used as catalyst under similar conditions.

Leaching test

A photocatalytic reaction with py-etPMO-Co was carried out as indicated previously, but after 1 h the reaction mixture was filtered off with a nylon membrane filter (0.45μm) to remove the catalyst particles. Then, the clear solution was transferred to a reaction tube under N_2 atmosphere and irradiated during 2 h.

Catalyst re-activation process

After reaction, the catalyst was recovered by centrifugation and washed with methanol and acetonitrile in order to eliminate possible residues of Eosin Y and TEOA in the pores. The re-activation process was similar to that used to anchor cobaloxime complex in py-etPMO material.

Characterization

X-ray powder diffraction (XRD) patterns were collected on a Bruker D8 Discover A25 diffractometer using Cu Kα radiation. N_2 adsorption-desorption isotherms were measured at -196 °C using an Autosorb-iQ MP/MP-XR instrument. Prior to measurement, all the samples were outgassed overnight at 120 °C. The surface area was calculated using the Brunauer-Emmett-Teller (BET) method and pore size distribution was determined using Density Functional Theory (DFT) method. Raman spectra of the samples were acquired with a Renishaw Raman instrument with green laser light (532 nm). FT-IR measurements were carried out on a Bruker Alpha II spectrometer. The solid-state ^{13}C CP/MAS NMR spectra were recorded on a Bruker Avance III HD 400 WB spectrometer at 13 kHz. An overall of 1500 free induction decays were accumulated for each measurement. The excitation pulse and recycle time for ^{13}C CP/MAS NMR were 3.6 ms and 2 s, respectively. Chemical shifts were referenced to tetramethylsilane (TMS) standard. X-ray photoelectron spectroscopy (XPS) were recorded on a SPECS Phoibos HAS 3500 150 MCD X-ray photoelectron spectrometer with a monochromatic Al anode (1486.7 eV). Accurate binding energies have been determined with respect to the porecosition of Si 2p at 103.4 eV. High-resolution Transmission Electron Microscopy images were recorded on a JEOL JEM 1400 microscope. Scanning Electron Microscopy imaging and Energy-dispersive X-ray (EDX) spectroscopy measurements were

performed on a JEOL JSM 7800F microscope. Inductively coupled plasma mass spectrometry (ICP-MS) for isotope ^{59}Co was measured using a NexION 350X spectrometer. Prior to the measurement, the sample was digested in an UltraWave microwave system.

Co K-edge x-ray absorption spectra were collected at the CLÆSS beamline of the ALBA synchrotron.[47] The synchrotron radiation was monochromatized by means of a double crystal Si(111) monochromator, while the higher harmonics were rejected by choosing proper angles and coatings for the collimating and focusing mirrors. The absorption data were acquired in transmission mode. The powdered samples were mixed uniformly in a boron nitride matrix and pressed into pellets to ensure an absorption jump close to 1. Several scans were measured to ensure reproducibility and a good signal to noise ratio. The data treated by the Demeter package.[48]

Results and discussion

Characterization of the cobaloxime-PMO hybrid catalyst

The powder X-ray diffraction (PXRD) pattern of pyridine-functionalized ethylene-bridged PMO revealed three reflection peaks in the low-angle region ($2\theta < 5$) with lattice *d*-spacings of 49, 28 and 25 Å, respectively. These peaks can be indexed to (100), (110) and (200) reflections of a highly ordered 2D-hexagonal (*p6mm*) structure (Fig. 1a, blue line).[49] The unit cell parameter of the hexagonal lattice (a_0) was 57 Å. After the incorporation of $Co(dmgH)(dmgH_2)Cl_2$ complex, the resulting py-etPMO-Co material showed similar diffraction peaks to the parent material py-etPMO (Fig. 1a, red line). Transmission electron microscopy (TEM)

of py-etPMO (Fig. S1) corroborated a highly ordered arrangement of uniform pores. These uniform pore channels were retained after cobaloxime anchoring on the pyridine groups located on the pore surface of PMO (Fig. 1b). These results together with the well-resolved XRD patterns demonstrated the formation of a highly ordered mesostructure, which was preserved after the coordination of the cobalt complex on the pyridine ligands.

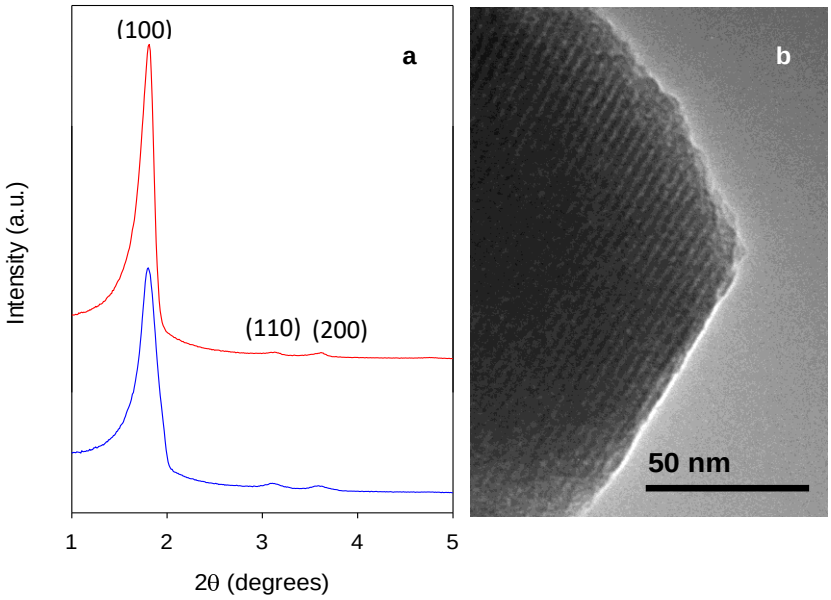

Fig 1. (a) PXRD of py-etPMO (blue) and py-etPMO-Co (red) and (b) TEM image of py-etPMO-Co.

Nitrogen adsorption-desorption isotherms of py-etPMO and py-etPMO-Co displayed a type-IV isotherm with a capillary condensation step at $P/P_0 = 0.3 – 0.6$, characteristic of mesoporous materials. Non-distinctive hysteresis loop was appreciated for both materials (Fig. 2). The BET surface area, pore volume and pore diameter are summarized in Table 1. The incorporation of the cobaloxime catalyst on the pore surface of py-etPMO caused a slight decrease of the S_{BET}, the pore volume and pore size values and a slight increase of the wall-thickness.

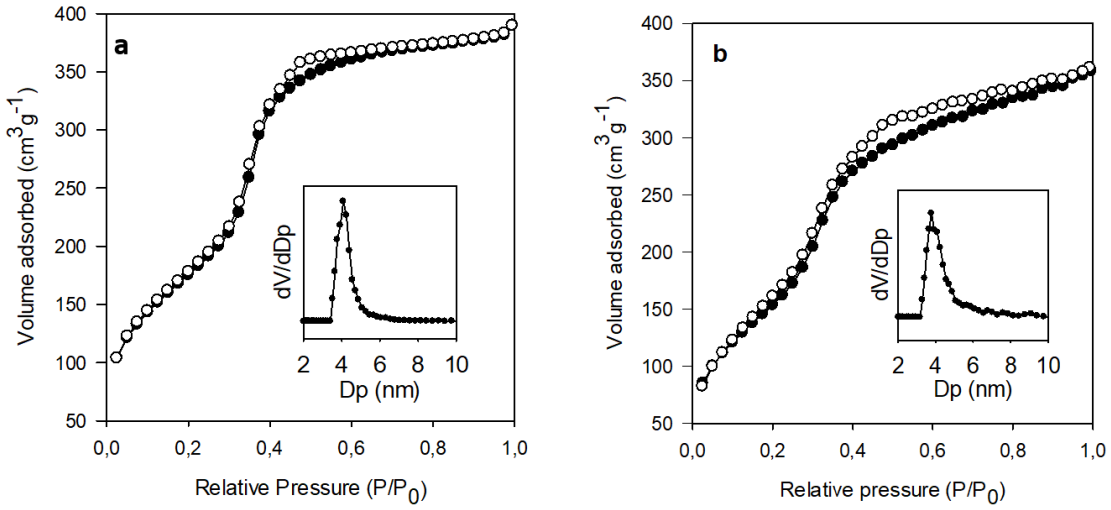

Fig 2. N_2 adsorption-desorption isotherms and pore size distributions (inset) of py-etPMO (a) and py-etPMO-Co materials (b).

Table 1. Physicochemical properties of periodic mesoporous organosilicas.

Sample	a_0[a] (nm)	S_{BET} (m^2/g)	V_p (cm^3/g)	D_p[b] (nm)	Wall thickness[c] (nm)
py-etPMO	5.7	683	0.55	4.1	1.6
py-etPMO-Co	5.6	651	0.51	3.8	1.8

[a] Unit cell parameter calculated $a_0 = \frac{2d_{100}}{\sqrt{3}}$,

[b] Calculated from DFT-analysis

[c] Calculated from the difference between a_0 and D_p

The presence of ethylene bridges as well as pyridylethyl moieties in the silica framework of PMO was confirmed by ^{13}C CP/MAS NMR measurements (Fig. 3 and Fig. S2). An intense signal centered at 5 ppm corresponded to the sp^3 carbon atoms of the ethylene bridges.[50] In addition, signals at 20, 30, 123 and 148 ppm were due to the pyridylethyl moieties incorporated on the channel pores.[49] A remaining signal at 58 ppm was associated to nonhydrolyzed ethoxy groups (-OCH_2CH_3) from the organosilane precursors. After incorporation of the

cobaloxime complex on the pore surface of py-etPMO, new signals appeared at 158 and 13 ppm associated to the C=N and CH_3 groups, respectively, from the glyoximate ligand.[51,52] Additional signals at 40 and 50 ppm were attributed to residual DMSO and CH_3OH used to remove unreacted cobaloxime complex after the immobilization process.[53]

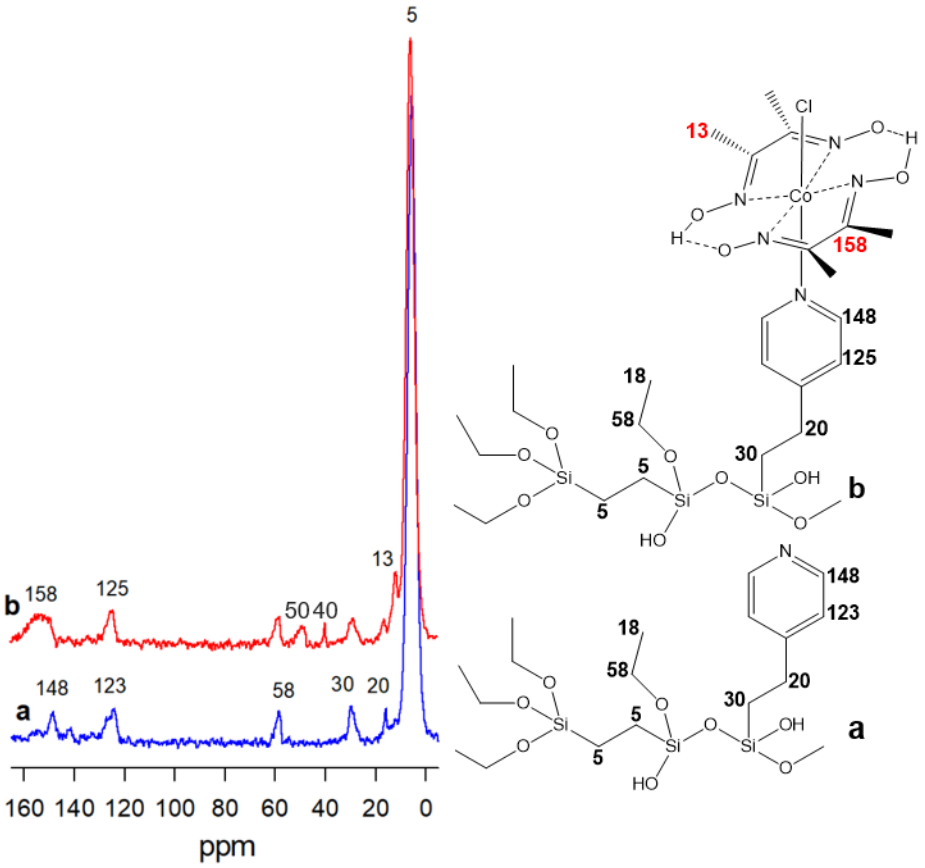

Fig 3. ^{13}C CP/MAS NMR spectra of py-etPMO (a) and py-etPMO-Co (b).

Raman and IR measurements further corroborated the presence of the cobaloxime at the pore surface of the py-etPMO. Raman spectrum of py-etPMO showed a peak at 3100 cm^{-1} attributed to the =C-H stretching vibrations from the pyridine ring. Several signals in the region of 1500–1600 cm^{-1} were assigned to the C=C stretching of heteroaromatic rings. After cobaloxime coordination, additional vibration modes at 1650 and 1220 cm^{-1} were related to C=N and N-O stretching,

respectively, of the cobaloxime catalyst (Fig. 4).[52] FT-IR results evidenced the coordination of cobalt on pyridine groups located on the PMO surface. Small vibration signals characteristic of the cobaloxime with axial pyridine ligands were observed at 1247 (νN-O) and 515 (νCo-N) cm^{-1} (Fig S3).[54–56]

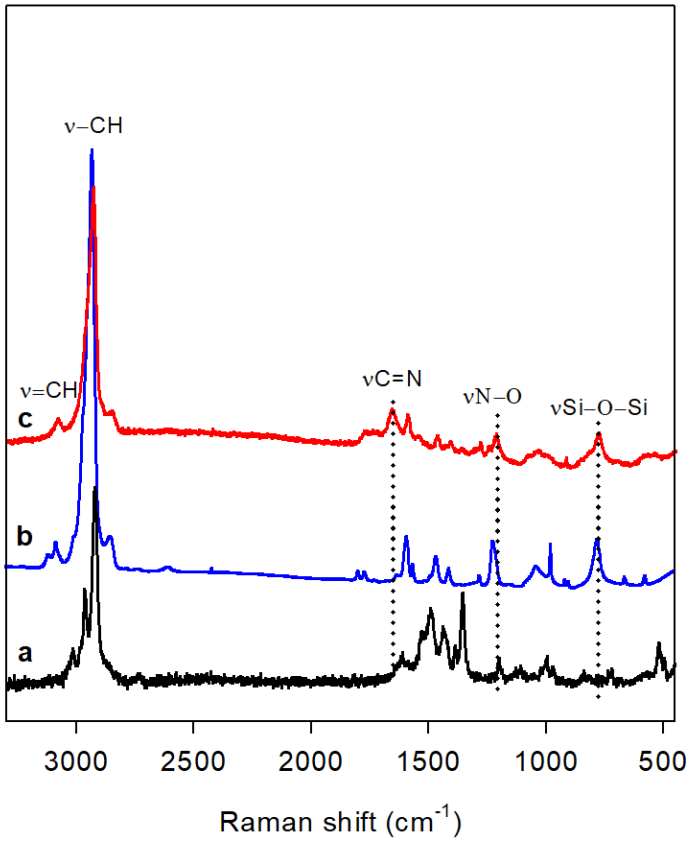

Fig 4. Raman spectra of $Co(dmgH_2)(dmgH)Cl_2$ complex (a), py-etPMO (b) and py-etPMO-Co (c).

Analysis of the samples by X-ray photoelectron spectroscopy (XPS) provided additional evidence of the successful immobilization of the cobaloxime complex on the PMO material. Survey spectrum of py-etPMO showed the presence of Si, C, N and O elements at the surface. Additional peaks associated to Co and Cl elements from cobaloxime units were present in the survey spectrum of py-etPMO-Co (Fig. S4). High-resolution N1s core of py-etPMO showed two nitrogen

contributions at 401.0 and 404.5 eV, which could be ascribed to pyridyl and protonated-pyridyl nitrogens of the pyridylethyl moieties in the silica framework of PMO, respectively (Fig. 5 (a)). Protonated-pyridyl nitrogens (+H-N-pyridinic) could be generated during the removal template under acidic conditions. For py-etPMO-Co, only a contribution centered at 401.2 eV was present. This peak would encompass contributions of the pyridyl nitrogen coordinated and non-coordinated to the Co centers as well as the glyoximate ligands of the cobaloxime.[57] Co 2p core region for py-etPMO-Co exhibited two signals centered at 781.5 eV ($2p_{3/2}$) and 796.5 ($2p_{1/2}$) eV in a 2:1 ratio (Fig. 5 (b)). The splitting of 15.0 eV and the lack of shake-up satellite bands clearly evidenced the presence of cobalt in +3 oxidation state.[58] These results are consistent with previous reports on cobaloxime grafted on semiconductors[57] or carbon nanotubes.[59]

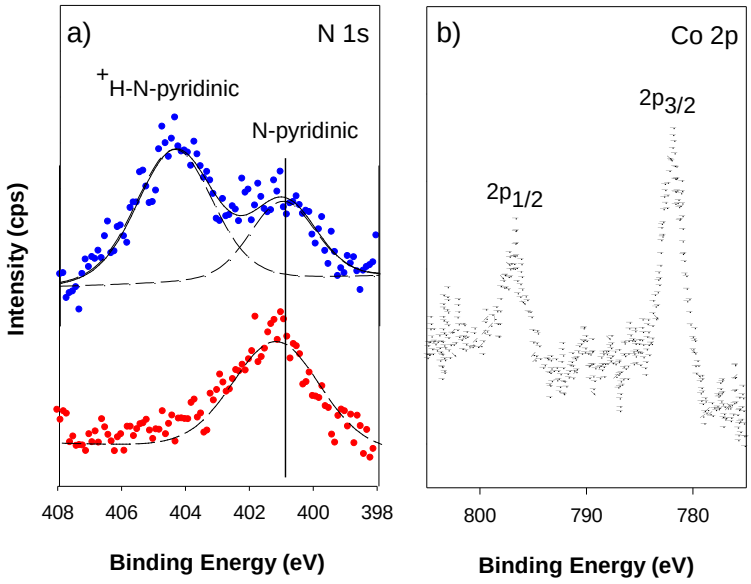

Fig 5. (a) N1s core level XPS spectra of py-etPMO (blue) and py-etPMO-Co (red). (b) Co2p core level XPS spectrum of py-etPMO-Co.

The pyridine content in the PMO support, py-etPMO, was analyzed by elemental analysis (Table S1). Based on the elemental analysis results, the nitrogen content was 0.41 mmol g^{-1}. Furthermore, the cobaloxime loading incorporated on the pore surface of py-etPMO-Co was 0.16 mmol Co per gram of catalyst. Accordingly, the cobaloxime/nitrogen ratio on py-etPMO-Co catalyst was 0.4. It means that approximately half of pyridine groups pendant on the PMO were coordinated to the cobaloxime complex, leaving uncoordinated pyridines available to recoordinate cobaloxime units during the photocatalytic experiments.[60] The incorporated cobaloximes were homogeneously distributed throughout the py-etPMO-Co particles according to SEM-EDX (Fig. S5).

In order to assure that coordination of the cobaloxime complexes occurs on the pendant pyridine units located on the PMO surface, an ethylene-bridged periodic mesoporous organosilica containing only ethane moieties in the silica walls[58] has been synthetized (see ESI for ethylene-bridged PMO synthesis). This material was dispersed in CH_3OH and stirred at 65 ºC overnight in the presence of $Co(dmgH_2)(dmgH)Cl_2$ complex. The negligible amount of cobalt in the resulting material by ICP-MS (0.792 x 10^{-3} mmol of Co per mg of material) clearly confirmed that only pyridine ligands on py-etPMO act as attachment points to assemble cobaloxime catalyst.

Co K-edge x-ray absorption spectroscopy (XAS) has been exploited to access the local electronic and structural properties around the cobalt centers. Figure 6 panel a depicts the x-ray absorption near edge structure (XANES), while panel b and c show the k^2 weighted extended x-ray absorption fine structure (EXAFS) oscillations and their relative Fourier. The XANES region is consistent with Co^{3+} oxidation state and its overall edge shape indicates an octahedral local

structure, with the spectral differences corresponding to change in the ligands and distortions. Both the reported XANES and EXAFS signals are in good agreement with the crystal structure of cobaloxime complex. More in particular, both the spectral features around 8 $Å^{-1}$ in the *k* and 1.9 Å in the R spaces are signature of a similar local environment.[61]

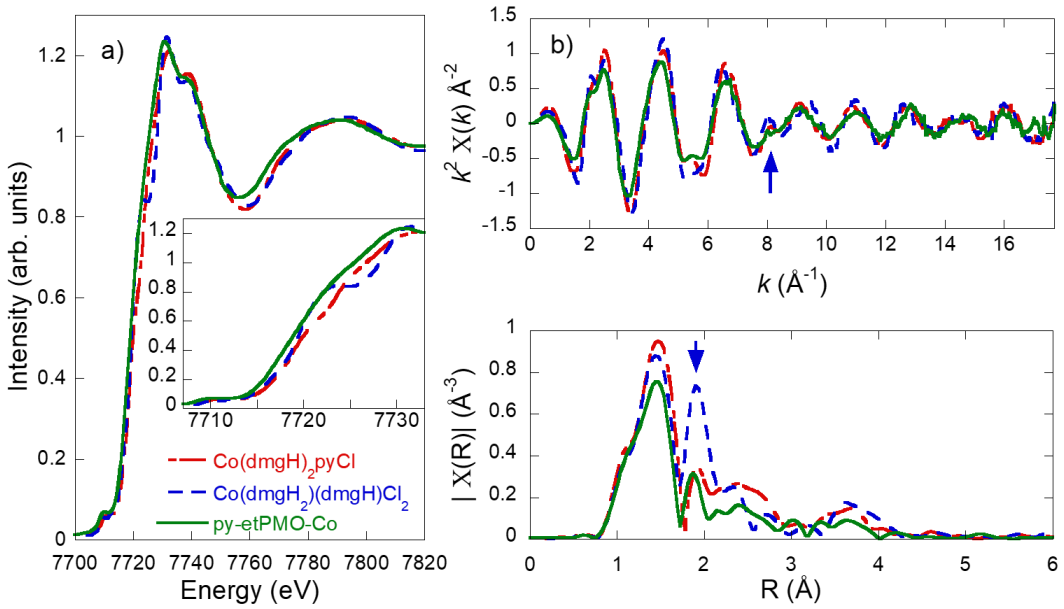

Fig 6. (a) Co K-edge XANES spectra collected over py-etPMO-Co, $Co(dmgH)_2pyCl$ and $Co(dmgH_2)(dmgH)Cl_2$ samples. The inset shows a zoom on the rising edges. (b) k^2 weighted EXAFS oscillations and (c) their relative Fourier transforms obtained from the 2.9-16.4 $Å^{-1}$ *k* range. The arrows highlight the spectral features characterizing the apical bonds (Co-Cl or Co–N (py)).

Catalytic activity

The potential of py-etPMO-Co as catalyst for the hydrogen evolution reaction was investigated in a visible light-activated system in the presence of a photosensitizer and a sacrificial electron donor. In this work, eosin Y (EY) and triethanolamine (TEOA) were chosen since they are commonly used when cobaloximes are essayed

for HER (Scheme 3).[25,47,50] All components present in the water reduction – sacrificial electron donor, photosensitizer and catalyst – are necessary to drive hydrogen evolution reaction.

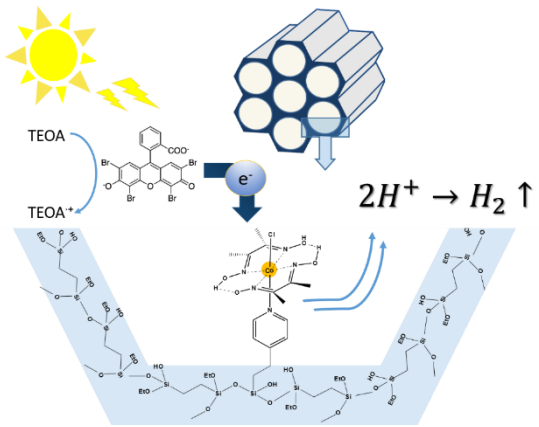

Scheme 3. Schematic representation of photocatalytic hydrogen production with py-etPMO-Co as catalyst.

In a typical photocatalytic experiment, py-etPMO-Co (1 mg) was suspended into the nitrogen purged CH_3CN:H_2O (1:1) solution containing EY (0.05 mM) and TEOA (4.29 mmol) ([EY]:[Co] = 3.75). Upon irradiation with visible light (>400 nm), the hydrogen evolving activity of the catalyst was examined by monitoring the headspace gas by GC at different time intervals. Preliminary studies were performed to optimize the EY concentration in our light-driven catalytic system (Fig S6).

The photocatalytic activity of py-etPMO-Co under conditions previously mentioned is shown in Fig. 6a. As can be observed, the HER was levelled off after 4 h irradiation with an initial H_2 evolution rate of 3.54 mmol h^{-1} g^{-1}. This corresponds to a hydrogen production maximum of ~18 mmol with a TON of 113. This H_2 production value largely exceeded that reported by Ott et col.[34] for a cobaloxime catalyst immobilized on MIL-101(Cr) under similar light-driven conditions where a TON of 18 was obtained at similar irradiation times. Therefore, we can hypothesize that the studied ordered mesoporous system provides an

improved accessibility of all components to the cobaloxime centers for the hydrogen production. Furthermore, compared to other heterogenized molecular HER catalysts reported in the literature, our py-etPMO-Co catalyst is among the most active systems for light-driven hydrogen evolution (Table S2).

Control tests were performed to confirm the key role of all components -*EY, catalyst, TEOA and light*- for photocatalytic HER. For all cases, the absence of one component in the light-driven system evolved a negligible amount of hydrogen (Fig. 7b). Similarly, no hydrogen was detected when py-etPMO-Co was substituted with py-etPMO.

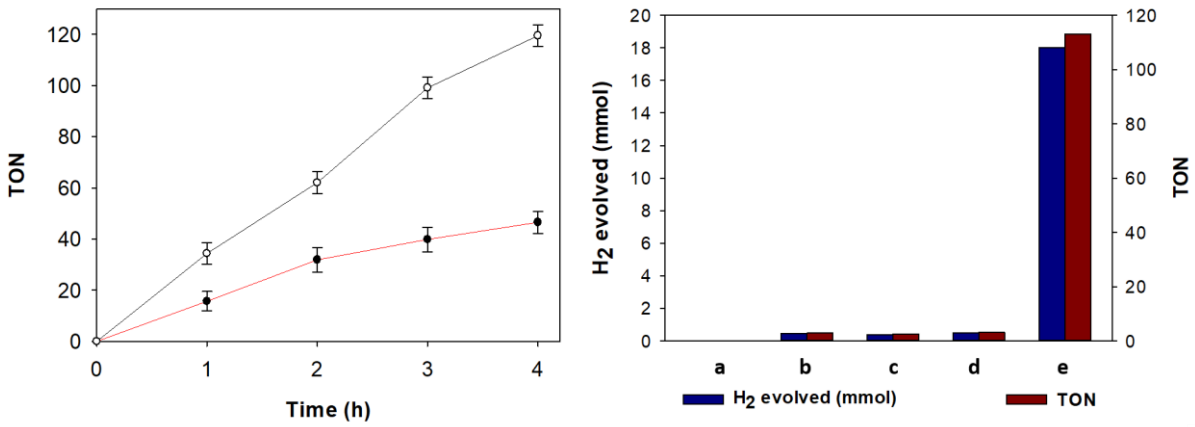

Fig 7. (a) Photocatalytic proton reduction with py-etPMO-Co (black) and $Co(dmgH)_2pyCl$ (red) as catalysts. (b) Control tests for py-etPMO-Co in HER without one component: light (a), TEOA (b), EY (c) and catalyst (d), compared to the HER system with all components (e).

Additionally, a leaching test was undertaken to assure that the hydrogen production reaction occurred heterogeneously by the cobaloxime catalyst anchored on the PMO mesochannels. After catalyst removal, the hydrogen evolution reaction

did not proceed, thus confirming that hydrogen production was not catalyzed by active homogeneous cobaloxime species leached out from py-etPMO-Co (Fig. S7).

However, after photocatalytic experiments, ICP-MS (0.034 μmol Co per mg) and XPS measurements (Fig. S8) of py-etPMO-Co material reflected that the cobaloxime complex was released from the mesoporous support during the H_2 production process. These findings were consistent with previous studies reported on electro- and photocatalytic HER that have questioned the stability of the pyridine-cobalt axial bond in the Co(I) oxidation state during the photocatalytic experiment. [28,31,34,65] A weak linkage between the Co(I) and the pyridine grafted on the PMO surface could be responsible of the leaching of the cobaloxime complex to the solution during the reaction. In order to prove that the cobalt center is detached to the axial pyridine ligands, py-etPMO-Co catalyst after photocatalytic reaction was collected and reactivated after treatment with $Co(dmgH_2)(dmgH)Cl_2$ complex. After that, the reactivated catalyst was collected and washed thoroughly with methanol and acetonitrile to remove any uncoordinated cobaloxime. ICP-MS analysis of the reactivated py-etPMO-Co catalyst gave 0.15 mmol Co per mg, similarly to the fresh catalyst, confirming the almost total restoration of the starting material. The reactivated catalyst was evaluated in HER under identical conditions than fresh catalyst, and it showed a comparable photocatalytic activity with a TON value of 110 after 4 h irradiation (Fig. 8). After a second reactivation treatment, the py-etPMO-Co maintained the initial activity. These results revealed that the hydrogen production is catalyzed by the cobaloxime catalyst immobilized on the pore surface of the PMO hybrid material, which can be restored to its initial activity during two recycling cycles. This total restoration of the catalytic activity of the PMO material was remarkable since the cobaloxime anchored on MIL-101

reported by Ott et col.[66]achieved approximately 60 % of its initial activity. These results evidence the good accessibility of the pyridine ligands positioned in the mesochannels of PMO, therefore facilitating its total restoration during the recycling tests.

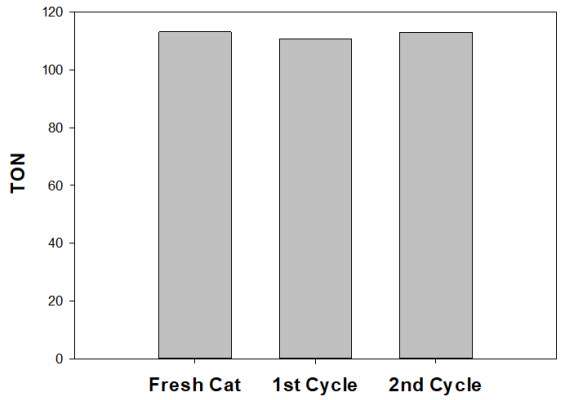

Fig 8. Recycling tests on py-etPMO-Co during 4 h

Furthermore, structural and textural properties of the py-etPMO-Co after photocatalysis were preserved, which confirmed the high mesostructural stability of the material under the photocatalytic conditions employed (Fig. 9). Clearly, the high hydrophobicity of the PMO framework determines its good stability in aqueous media.[37,58]

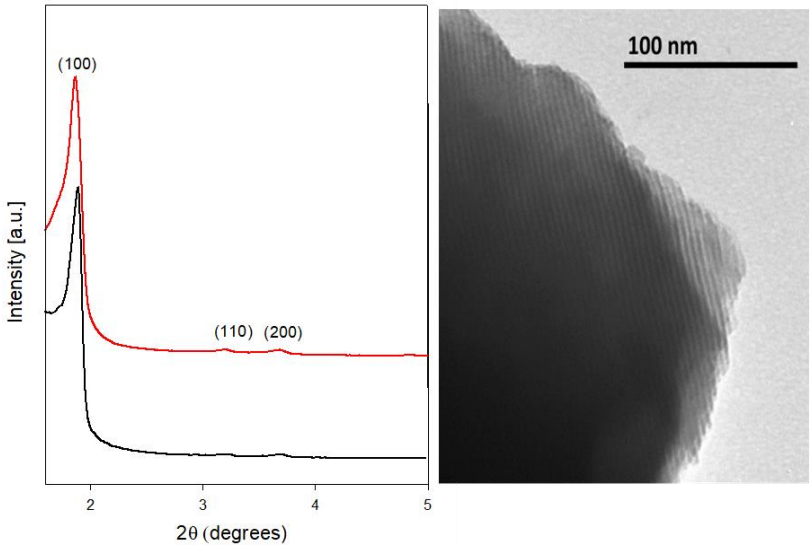

Fig 9. (a) PXRD of py-etPMO-Co before (red) and after (black) photocatalysis (b) TEM image of py-etPMO-Co after photocatalytic reaction.

Conclusions

A novel cobaloxime-PMO hybrid material was prepared via complexation of cobaloxime units on the pyridine moieties present on the surface of an ethylene-bridged PMO material. This strategy allows obtaining an efficient hydrogen evolving catalyst in presence of EY as photosensitizer and TEOA as sacrificial electron donor, achieving a TON of 113. This system shows an enhanced photocatalytic performance under the studied conditions in comparison to its homogeneous counterpart, which suggests an increased stability of the cobaloxime catalyst confined into the mesopores. Although this system was able to restore its initial catalytic activity during two recycling experiments, a previous reactivation process was needed to coordinate cobaloxime centers on the PMO material. These results confirm that its applicability during continuous photocatalytic processes is still limited due to the inherent instability of the cobalt-pyridine axial bond during the photocatalytic

reaction. Future studies are being addressed to enhance the photocatalytic stability of Co-py linkages on PMO mesochannels.

Conflicts of Interest

The authors declare no conflict of interest.

Acknowledgements

The authors are grateful to Ramon Areces Foundation, Spanish Ministry of Science, Innovation and Universities (Project RTI2018-101611-B-I00) and Feder Funds for financial support. The technical support from IUIQFN and SCAI are greatly appreciated. A. B. acknowledges the DST-INSPIRE program for an INSPIRE Faculty Fellowship (DST/INSPIRE/04/2017/001072).

References

1 T. Lauvaux, K. R. Gurney, N. L. Miles, K. J. Davis, S. J. Richardson, A. Deng, B. J. Nathan, T. Oda, J. A. Wang, L. Hutyra and J. Turnbull, *Environ. Sci. Technol.*, 2020, **54**, 10237–10245.

2 N. S. Lewis and D. G. Nocera, *Proc Natl Acad Sci U S A*, 2006, **103**, 15729–15736.

3 K. L. Bren, *Interface Focus*, 2015, **5**, 1–12.

4 I. E. A. Pvps, A. Report, P. Power and S. Programme, *Int. Energy Agency Photovolt. Power Syst. Program.*, 2020.

5 N. Abas, E. Kalair, A. Kalair, Q. ul Hasan and N. Khan, *Int. J. Hydrogen Energy*, 2020, **45**, 20787–20799.

6 T. Keijer, T. Bouwens, J. Hessels and J. N. H. Reek, *Chem. Sci.*, 2021, **12**, 50–70.

7 R. Eisenberg and H. B. Gray, *Inorg. Chem.*, 2008, **47**, 1697–1699.

8 P. Du and R. Eisenberg, *Energy Environ. Sci.*, 2012, **5**, 6012–6021.

9 M. W. Kanan, J. Yano, Y. Surendranath, M. Dinca, V. K. Yachandra and D. G. Nocera, *J. Am. Chem. Soc.*, 2010, **132**, 13692–13701.

10 Q. Yin, J. M. Tan, C. Besson, Y. V Geletii, D. G. Musaev, A. E. Kuznetsov, Z. Luo, K. I. Hardcastle and C. L. Hill, *Science (80-.).*, 2010, **328**, 342–346.

11 W. R. Mcnamara, Z. Han, P. J. Alperin, W. W. Brennessel, P. L. Holland and R. Eisenberg, *J. Am. Chem. Soc.*, 2011, **133**, 15368–15371.

12 B. D. Stubbert, J. C. Peters and H. B. Gray, *J. Am. Chem. Soc.*, 2011, **133**, 18070–18073.

13 J. L. Dempsey, B. S. Brunschwig, J. R. Winkler and H. B. Gray, *Acc. Chem. Res.*, 2009, **42**, 1195–2004.

14 V. Artero, M. Chavarot-Kerlidou and M. Fontecave, *Angew. Chemie - Int. Ed.*, 2011, **50**, 7238–7266.

15 M. Natali, A. Luisa, E. Iengo and F. Scandola, *Chem. Commun.*, 2014, **50**, 1842–1844.

16 N. Kaeffer, M. Chavarot-Kerlidou and V. Artero, *Acc. Chem. Res.*, 2015, **48**, 1286–1295.

17 D. Dolui, S. Khandelwal, P. Majumder and A. Dutta, *Chem. Commun.*, 2020, **56**, 8166–8181.

18 J. Hawecker, J. Lehn and R. Ziessel, *J. Chem. Soc., Chem. Commun*, 1983, 536–538.

19 S. R. Soltau, J. Niklas, P. D. Dahlberg, O. G. Poluektov, D. M. Tiede, K. L. Mulfort and L. M. Utschig, *Chem. Commun.*, 2015, **51**, 10628–10631.

20 F. Lakadamyali and E. Reisner, *Chem. Commun.*, 2011, **47**, 1695–1697.

21 M. Razavet, V. Artero and M. Fontecave, *Inorg. Chem.*, 2005, **44**, 4786–4795.

22 D. W. Wakerley and E. Reisner, *Phys. Chem. Chem. Phys.*, 2014, **16**, 5739–5746.

23 A. Panagiotopoulos, K. Ladomenou, D. Sun, V. Artero and A. G. Coutsolelos, *Dalt. Trans.*, 2016, **45**, 6732–6738.

24 D. Dolui, S. Khandelwal, A. Shaik, D. Gaat, V. Thiruvenkatam and A. Dutta, *ACS Catal.*, 2019, **9**, 10115–10125.

25 Y. K. Jiang and J. H. Liu, *Int. J. Quantum Chem.*, 2012, **112**, 2541–2546.

26 A. Kahnt, K. Peuntinger, C. Dammann, T. Drewello, R. Hermann, S. Naumov, B. Abel and D. M. Guldi, *J. Phys. Chem. A*, 2014, **118**, 4382–4391.

27 J. Chen and P. H. L. Sit, *ACS Omega*, 2019, **4**, 582–592.

28 N. M. Muresan, J. Willkomm, D. Mersch, Y. Vaynzof and E. Reisner, *Angew. Chemie - Int. Ed.*, 2012, **51**, 12749–12753.

29 B. Reuillard, J. Warnan, J. J. Leung, D. W. Wakerley and E. Reisner, *Angew. Chemie - Int. Ed.*, 2016, **55**, 3952–3957.

30 E. S. Andreiadis, P. A. Jacques, P. D. Tran, A. Leyris, M. Chavarot-Kerlidou, B. Jousselme, M. Matheron, J. Pécaut, S. Palacin, M. Fontecave and V. Artero, *Nat. Chem.*, 2013, **5**, 48–53.

31 S. Donck, J. Fize, E. Gravel, E. Doris and V. Artero, *Chem. Commun.*, 2016, **52**, 11783–11786.

32 B. L. Wadsworth, A. M. Beiler, D. Khusnutdinova, S. I. Jacob and G. F. Moore, *ACS Catal.*, 2016, **6**, 8048–8057.

33 C. Tapia, E. Bellet-Amalric, D. Aldakov, F. Boudoire, K. Sivula, L. Cagnon and V. Artero, *Green Chem.*, 2020, **22**, 3141–3149.

34 S. Roy, A. Bhunia, N. Schuth, M. Haumann and S. Ott, *Sustain. Energy Fuels*,

2018, **2**, 1148–1152.

35 S. Roy, Z. Huang, A. Bhunia, A. Castner, A. K. Gupta, X. Zou and S. Ott, *J. Am. Chem. Soc.*, 2019, **141**, 15942–15950.

36 K. Gottschling, G. Savasci, H. Vignolo-González, S. Schmidt, P. Mauker, T. Banerjee, P. Rovó, C. Ochsenfeld and B. V. Lotsch, *J. Am. Chem. Soc.*, 2020, **142**, 12146–12156.

37 P. Van Der Voort, D. Esquivel, E. De Canck, F. Goethals, I. Van Driessche and F. J. Romero-salguero, *Chem. Soc. Rev.*, 2013, **42**, 3913–3955.

38 D. Esquivel, E. Canck, C. Jimenez-Sanchidrian, P. Voort and F. Romero-Salguero, *Curr. Org. Chem.*, 2014, **18**, 1280–1295.

39 D. Esquivel, E. De Canck, C. Jiménez-Sanchidrián, P. Van Der Voort and F. J. Romero-Salguero, *J. Mater. Chem.*, 2011, **21**, 10990–10998.

40 W. J. Hunks and G. A. Ozin, *Chem. Commun.*, 2004, 2426–2427.

41 N. Mizoshita, T. Tani and S. Inagaki, *Chem. Soc. Rev.*, 2011, **40**, 789–800.

42 A. M. Kaczmarek, S. Abednatanzi, D. Esquivel, C. Krishnaraj, H. S. Jena, G. Wang, K. Leus, R. Van Deun, F. J. Romero-Salguero and P. Van Der Voort, *Microporous Mesoporous Mater.*, 2020, **291**, 109687.

43 T. Himiyama, M. Waki, D. Esquivel, A. Onoda, T. Hayashi, P. Van Der Voort and S. Inagaki, *ChemCatChem*, 2018, **10**, 4908–4913.

44 W. C. Trogler and R. C. Stewart, *Inorg. Chem.*, 1974, **13**, 1564–1570.

45 M. Waki, N. Mizoshita, T. Tani and S. Inagaki, *Angew. Chemie-International Ed.*, 2011, **50**, 11667–11671.

46 A. M. Kaczmarek, D. Esquivel, B. Laforce, L. Vincze, P. Van Der Voort, F. J. Romero-Salguero and R. Van Deun, *Luminescence*, 2018, **33**, 567–573.

47 L. Simonelli, C. Marini, W. Olszewski, M. Á. Pérez, N. Ramanan, G. Guilera

and V. Cuartero, *Cogent Phys.*, 2016, **3**, 1–10.

48 B. Ravel and M. Newville, *J. Synchrotron Rad.*, 2005, **12**, 537–541.

49 M. Waki, N. Mizoshita, T. Ohsuna, T. Tani and S. Inagaki, *Chem. Commun.*, 2010, **46**, 8163–8165.

50 M. I. López, D. Esquivel, C. Jiménez-Sanchidrián, F. J. Romero-Salguero and P. Van Der Voort, *J. Catal.*, 2015, **326**, 139–148.

51 T. Banerjee, F. Haase, G. Savasci, K. Gottschling, C. Ochsenfeld and B. V. Lotsch, *J. Am. Chem. Soc.*, 2017, **139**, 16228–16234.

52 D. A. Thornton, *Coord. Chem. Rev.*, 1990, **104**, 251–295.

53 G. R. Fulmer, A. J. M. Miller, N. H. Sherden, H. E. Gottlieb, A. Nudelman, B. M. Stoltz, J. E. Bercaw and K. I. Goldberg, *Organometallics*, 2010, **29**, 2176–2179.

54 G. F. M. Alexandra Krawicz, Jinhui Yang, Eitan Anzenberg, Junko Yano, Ian D. Sharp, *J. Am. Chem. Soc.*, 2013, **135**, 11861–11868.

55 A. Panagiotopoulos, K. Ladomenou, D. Sun, V. Artero and A. G. Coutsolelos, *Dalt. Trans.*, 2016, **45**, 6732–6738.

56 T. J. Chuang, C. R. Brundle and D. W. Rice, *Surf. Sci.*, 1976, **59**, 413–429.

57 A. Krawicz, J. Yang, E. Anzenberg, J. Yano, I. D. Sharp and G. F. Moore, *J. Am. Chem. Soc.*, 2013, **135**, 11861–11868.

58 D. Esquivel, C. Jiménez-Sanchidrián and F. J. Romero-Salguero, *Mater. Lett.*, 2011, **65**, 1460–1462.

59 S. Donck, J. Fize, E. Gravel, E. Doris and V. Artero, *Chem. Commun.*, 2016, **52**, 11783–11786.

60 M. Gruttadauria, F. Giacalone and R. Noto, *Green Chem.*, 2013, **15**, 2608–2618.

61 S. Roy, A. Bhunia, N. Schuth, M. Haumann and S. Ott, *Sustain. Energy Fuels*, 2018, **2**, 1148–1152.

62 T. M. McCormick, B. D. Calitree, A. Orchard, N. D. Kraut, F. V. Bright, M. R. Detty and R. Eisenberg, *J. Am. Chem. Soc.*, 2010, **132**, 15480–15483.

63 E. Edwards, R. Roychoudhury, B. Schwarz, P. Jordan, J. Lisher, M. Uchida and T. Douglas, *J. Mater. Chem. B*, 2016, **4**, 5375–5384.

64 T. Lazarides, T. Mccormick, P. Du, G. Luo, B. Lindley and R. Eisenberg, *J. Am. Chem. Soc.*, 2009, **131**, 9192–9194.

65 J. Willkomm, N. M. Muresan and E. Reisner, *Chem. Sci.*, 2015, **6**, 2727–2736.

66 S. Roy, A. Bhunia, N. Schuth, M. Haumann and S. Ott, *Sustain. Energy Fuels*, 2018, **2**, 1148–1152.